NUMERICAL ANALYSIS OF THE INFLUENCE OF AIR COMPRESSIBILITY EFFECTS ON THE OSCILLATING WATER COLUMN WAVE ENERGY CONVERTER CHAMBER

Rafael Adriano Alves Camargo Gonçalves

Paulo Roberto de Freitas Teixeira

rafaelcamagon@bol.com.br

prfreitasteixeira@gmail.com

Universidade Federal do Rio Grande

Av. Itália, km 8, 96201-900, Rio Grande, Brazil

Eric Didier

edidier@lnec.com

Laboratório Nacional de Engenharia Civil – LNEC

Av. do Brasil 101, 1700-066, Lisbon, Portugal

Fernando Ramos Torres

ftorres571@gmail.com

Universidade Federal do Rio Grande

Abstract. *The most studied device used for extracting wave energy is the Oscillating Water Column (OWC). In general, numerical simulations of these cases by means of models based on Reynolds-Averaged-Navier-Stokes (RANS) equations adopt the Volume of Fluid (VoF) method to take into account the water and air whose flows are incompressible. The aim of this study is to investigate the influence of the compressibility effect on the air inside the chamber by means of FLUENT® numerical model. Both water and air flows are still considered incompressible, but, at every instant, a pressure based on an analytical equation that takes into account the turbine characteristic relation (k_t) of a Wells turbine and the isentropic transformation of the air is imposed on the top boundary of the chamber. Incident waves with period of 9 s and 1 and 2 m high are imposed in a flume 10 m deep with an onshore OWC at its end ($k_t = 240$ Pa s m^{-3}). Results show differences between incompressible and compressible air around 12% in the air pressure amplitude inside the chamber and about 21% in the average pneumatic power.*

Keywords: *Wave energy, Oscillating Water Column device, Numerical simulation, Finite volume method, Volume of Fluid*

1 INTRODUCTION

The fossil fuels are the main energy source of the world that will represent around 80% of the total energy in 2030 (International Energy Agency, 2008). Their excessive use cause several problems, including the greenhouse effect. Therefore, studies about exploitation of clean and renewable energies are fundamental. Sea waves are an alternative, due to their natural and periodic phenomena and the larger amount of available energy in the oceans, estimated in 32 TW/year (Mørk et al., 2010).

The aggressive environment that the wave energy converter devices are subjected is their great disadvantage, requiring structures to resist corrosion and mechanical fatigue (Falcão, 2010). The variability of the energetic flux of the waves requires deep studies about device choice and its design, since parameters, such as height and wave length are temporal and spatial variables.

Oscillating Water Column (OWC) devices are the most developed one (Falcão, 2002), due to their constructive and maintenance advantages. The concept of the OWC device was created by Yoshio Masuda, in the middle of the 20th century (Falcão and Henriques, 2015). Later, research and development programs in renewable energies allowed the construction of OWC prototype plants in several regions, such as in Pico Island, Portugal and in Islay Island, Scotland (Jossét and Clément, 2007). While offshore OWC's are floating and require a high cost of maintenance, onshore OWC's are fixed and generally can be design to be inserted in breakwaters. These devices consist in an air chamber, valves, ducts, turbine and electric generator. In fixed devices, the front wall of the chamber, composed by concrete or steel, is partially submerged (Falcão, 2010). The water flow, caused by the incident wave, makes the movement of the free surface inside the chamber and air compression and depression inside the chamber activate the turbine. The electric generator is coupled to the turbine axis and converts mechanical energy into electrical one.

Basically, turbines can be classified as reaction or impulse turbines (Pereiras et al., 2015). The choice of the turbine depends mainly on the sea state, but noise and maintenance are also important aspects to be considered (Falcão, 2015). Wells turbine belongs to reaction turbine group and it is most used in OWC devices (Setoguchi et al., 2001), since it is relatively simple and self-rectifying, i.e., it rotates in the same direction independently of flow direction (Falcão, 2010). The Wells turbine possesses higher peak efficiency and a narrower operating range in relation to the impulse turbine (Das et al, 2017). Frequently, valves are coupled in series or in parallel to enable optimal efficiency of the turbine (Raghunathan, 1995).

Models based on Reynolds averaged Navier-Stokes (RANS) equations are a good option to analyze the output power of an OWC wave energy converter numerically, since they take into account complex phenomena, such as viscosity effects, wave breaking and both nonlinear wave-structure interaction and hydro-aerodynamic coupling. Up to now, RANS models have been used for reaching this objective by some researchers, such as Horko, 2007; Liu et al., 2008, 2009a, 2009b; Marjani et al., 2008; López et al., 2014; Luo et al., 2014; Iturrioz et al., 2015; Kamath et al., 2015; Bouali and Larbi, 2017; and Lopez et al., 2016. In most studies, an orifice or/and a porous media are used to represent the air damping inside the chamber imposed by the turbine. However, Torres et al. (2016) show a methodology, by using the academic Fluinco model which takes into account the actual air damping of the Wells turbine, represented by a turbine characteristic relation (k_t) in which the pressure loss and the flow rate of the turbine are considered. By using the principle of similitude of turbomachinery, the authors conclude that k_t is related to the rotational speed and the diameter of the turbine. They

Proceedings of the XXXVIII Iberian Latin-American Congress on Computational Methods in Engineering
P.O. Faria, R.H. Lopez, L.F.F. Miguel, W.J.S. Gomes, M. Noronha (Editores), ABMEC, Florianópolis, SC, Brazil, November 5-8, 2017.

consider hydro-aerodynamic coupling, performance curves of the turbine and air pressure control by a relief valve.

In general, numerical simulations of these cases, by means of models based on RANS equations, adopt the Volume of Fluid (VoF) method to take into account the water and air, whose flows are incompressible. Therefore, the inherent thermodynamic transformation inside the chamber is not considered, leading to errors in the solution. Compressibility air effects can influence significantly the evaluation of the energy conversion of the OWC (Sheng, 2013). The use of the state equation allows results close to reality and explains energetic losses due to the air compressibility effects in OWC devices (Medina-López et al, 2017). However, this task is very difficult, because, even if some RANS models are able to consider the air flow as compressible, they demand high computational cost, due to the addition of the energy equation and the drastic decrease of the time step. To solve this difficulty, the aim of this study is to investigate the influence of the compressibility effect on the air inside the chamber by proposing an alternative approach: both water and air flows are still considered incompressible, but a methodology is used for imposing, on the top boundary of the chamber, at every instant, the air pressure based on an analytical equation that takes into account the turbine characteristic relation (k_t) of a Wells turbine and the isentropic transformation of the air. The FLUENT® numerical model is employed and User Defined Functions (UDF) are used for imposing wave generation and Wells turbine effect on the air chamber top boundary.

2 STUDY CASE

The study case consists in a flume 10 m deep with an OWC device at its end. The chamber is 6.0 m high, 10.0 m wide and 10.0 m long. The front wall is 0.5 m thick and is 2.5 m submerged. Figure 1 shows the scheme of the domain. Two incident waves, both with period T = 9 s and height H = 1 m and 2 m, are tested. The incident wave power that must be extracted can be evaluated by its time-average, P_w, as following (Dean and Dalrymple, 2000):

$$P_w = \left(\frac{1}{8}\rho g\, H^2\right)\frac{L}{T}\left[\frac{1}{2}\left(1+\frac{2kh}{\sinh 2kh}\right)\right]A \quad (1)$$

where g is the gravitational acceleration, T is the incident wave period, L is the wavelength, H is the wave height, $k = 2\pi/L$ is the wave number and A is the chamber width.

The pressure gradient through the rotor paddle of the turbine causes lift forces, which enables the transference of flow energy to the turbine axis. The Wells turbine has a linear relation between flow rate and pressure loss (Torres et al., 2015; Sheng and Lewis, 2016) as expressed by the following equation:

$$p = k_t\, Q_t \quad (2)$$

where p is the pressure, Q_t is the volumetric flow rate and k_t is the turbine characteristic relation, that is 240 Pa s m^{-3} in this study. The variability of the sea state can cause low efficiency of Wells turbines, because their operational power range is restricted by the lift loss of the rotor paddles (stall) (Torres et al., 2016; Brito-Melo et al., 2002). This difficulty can be avoided by using rotor velocity control or flow direction paddles. Figure 2 shows a scheme of the Wells turbine (Setoguchi and Takao, 2006).

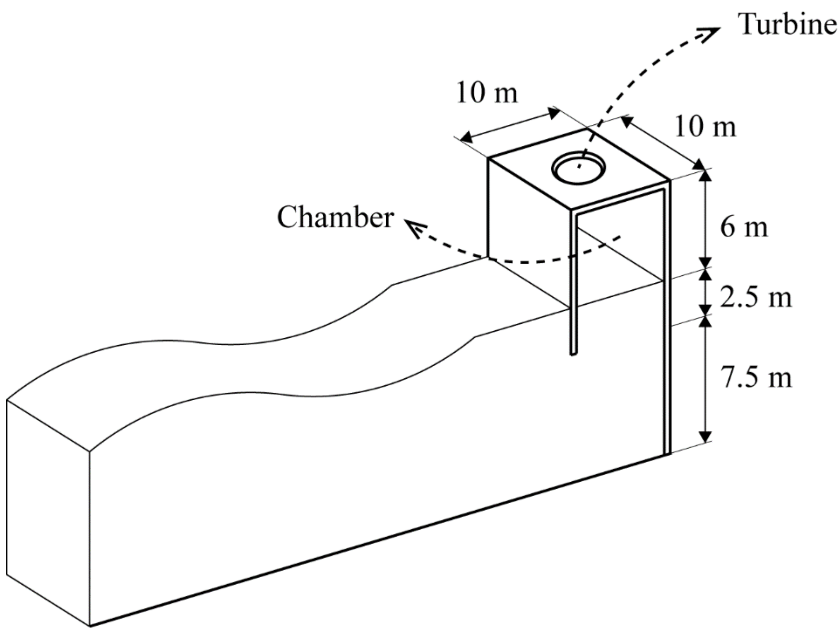

Figure 1. Scheme of the domain.

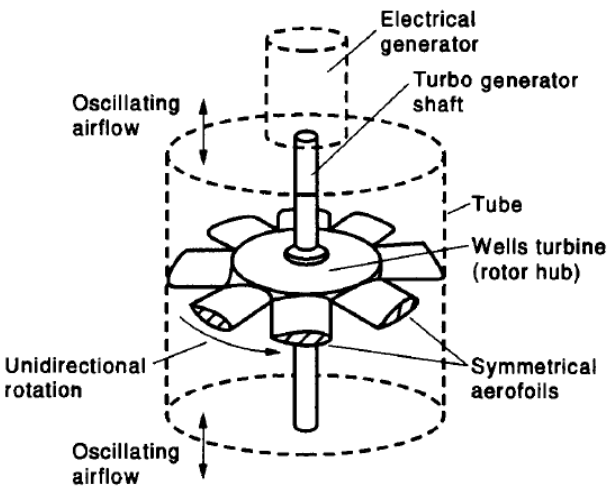

Figure 2. Scheme of the Wells turbine.

The mechanical power of the turbine depends on the available pneumatic power, rotational speed and turbine geometry (Torres et al., 2016). The pneumatic power is given by:

$$P_p = \frac{p^2}{k_t} \tag{3}$$

Its mean value ($\bar{P}_p$) can be calculated by integrating P_p in a wave period and dividing by the wave period.

3 METHODOLOGY

The equations that represent the phenomena, continuity and momentum, are given by:

$$\frac{\partial u_i}{\partial x_i} = 0 \tag{4}$$

$$\frac{\partial u_i}{\partial t} + u_i \frac{\partial u_i}{\partial x_j} = -\frac{1}{\rho}\frac{\partial p}{\partial x_i} + g_i + \frac{1}{\rho}\frac{\partial \tau_{ij}}{\partial x_j} \tag{5}$$

where i, j = 1, 2, t is the time, p is the pressure, ρ is the specific mass, g is the gravity acceleration and τ_{ij} is the viscous stress tensor. In this study, Reynolds-Average-Navier-Stokes (RANS) equations, based on the decomposition of the instantaneous velocity and pressure fields of the Navier–Stokes equations, Eqs. (4) and (5), into mean and fluctuating components, and the subsequent time-averaging of the set of equations, are used. This process introduces Reynolds stress terms associated with the turbulence. The standard k-ε turbulence model is used to relate Reynolds stresses to mean flow variables and close the equations.

Free surface flow motion is defined by the VoF method (Hirt and Nichols, 1981), which is based on the transport equation of the volume fraction, given by:

$$\frac{\partial \alpha}{\partial t} + u_j \frac{\partial \alpha}{\partial x_j} = 0 \tag{6}$$

where the volume fraction, α, is a scalar that takes the value 0 in the air, 1 in the water and, to identify the position of the free surface, the value 0.5.

The RANS-VOF numerical code Fluent, version 6.3.26 (Fluent, 2006), applies a Finite Volume technique to solve RANS and VoF equations, where variables are defined in the center of each control volume. The interaction among incident waves and the OWC device has predominantly a 2D hydrodynamic behavior. Therefore, a 2D numerical model, that demands lower computational cost than a 3D model, is used. However, the aerodynamic effect of the Wells turbine in the air chamber, particularly the pressure and its action on the free surface inside the OWC chamber, is 3D and, consequently, the flow rate at the turbine is calculated taking into account the width of the chamber (Torres et al., 2016), that is 10 m in this study. This methodology has been validated and applied to OWC wave converters by Paixão Conde et al., 2011; Didier et al., 2011; Teixeira et al., 2013; Dias et al., 2015; Mendonça et al., 2017.

The numerical Wells turbine is modeled by means of Eq. (2), which is imposed as boundary condition on the chamber top by using an UDF. The pressure (p), at each time, is calculated using the flow rate of the previous instant. The OWC chamber is considered an open system, because it allows the transition of mass through its boundaries. The control volume is limited by the free surface, walls and the turbine. The pressure is considered uniform in the volume control. A thermodynamic analysis of the air, taking into account an isentropic process, produces a mathematical relation that involves the flow rate, the specific mass and the pressure inside the chamber with the volumetric flow rate of the turbine, as follows (Jossét and Clément, 2007):

$$\frac{\dot{p}}{(p+p_o)} = -\gamma\left[\frac{Q_t}{V_c}\left(1-\varepsilon\frac{\rho-\rho_o}{\rho}\right)+\frac{\dot{V}_C}{V_c}\right] \tag{7}$$

$$\rho = \rho_o\left(\frac{p}{p_o}\right)^{\frac{1}{\gamma}} \tag{8}$$

where ρ_c and ρ_o are specific mass of the air inside the chamber and of the atmosphere, respectively; p and $\dot{p}$ are the air pressure and its rate; V_c and $\dot{V}_c$ are the volume of the air inside the chamber and its rate; and Q_t is the flow rate of the turbine. γ is the adiabatic expansion coefficient (1.4 for ideal gases) and ε is 1 for inhalation and null for exhalation.

Equations (7) and (2) are discretized in first order finite differences and, then, the pressure is imposed on the top boundary of the chamber (pressure outlet) at each instant by means of UDF (Fig. 3), taking into account the other variables obtained at previous instant (Teixeira et al., 2013). This methodology allows considering the air compressibility inside the chamber without the directly use of the energy equation to close the problem.

The wave generation is imposed on the paddle boundary, by means of UDF, considering a velocity inlet where components of velocity and elevation (phase) are those of linear wave theory (Dean and Dalrymple, 2000). Additionally, the active absorption method (Didier, 2017) is employed to be possible the use of a short flume and long time series of variables, such as pressure inside the chamber and free surface elevations. Non-slip condition is imposed on the bottom and chamber walls and atmosphere pressure is imposed on the top boundary of the flume (Fig. 3).

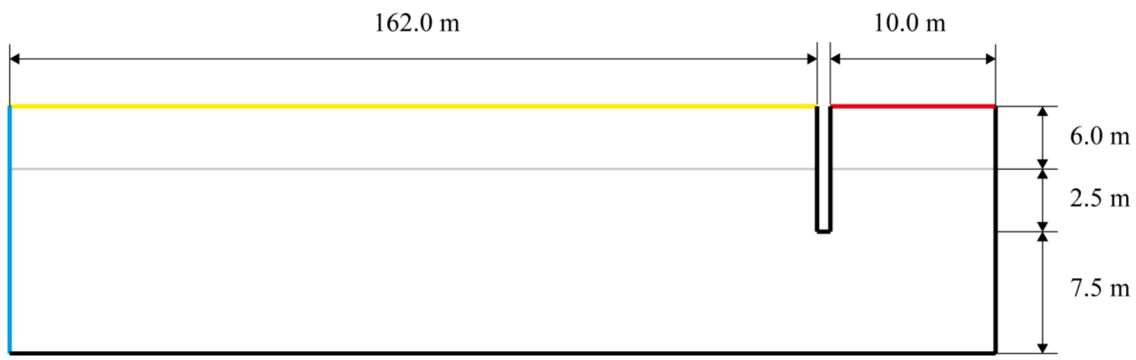

Figure 3. Computational domain. Bottom – black line, paddle – blue line, pressure outlet (atmosphere) – yellow line and turbine – red line.

In FLUENT® model, the *k*-e model is used for turbulence, with standard parameters. The solve scheme is SIMPLEC and the scheme PRESTO! is used to the pressure discretization. The momentum, turbulence kinetic energy and dissipation rate are discretized by the third-order scheme of MUSCL. The computational domain is spatially discretized by using regular meshes of quadrilateral cells (Fig. 4). There are 125 divisions in vertical direction, in which 50 are located in the zone where the free surface varies. In the horizontal direction, 390 divisions are adopted with maximum size of 70 cells per wavelength, wherein at beginning and inside the chamber the mesh is refined (Teixeira et al., 2013).

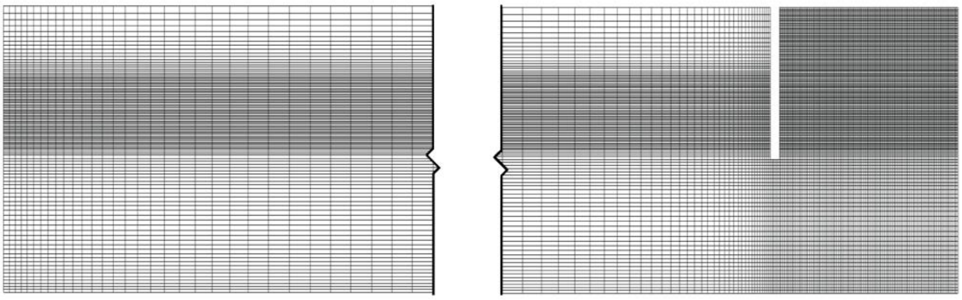

Figure 4. Mesh of the computational domain.

4 RESULTS AND DISCUSSIONS

Results of incompressible model and compressible one are compared in terms of temporal series of free surface elevation and pressure inside the chamber. The temporal series of elevation is a mean value along the length of the chamber and the temporal series of pressure is obtained by a gauge at 3 m from the still water level. Figure 5 shows the temporal series of the free surface elevation and the pressure inside the chamber for the incident wave with $T = 9$s and $H = 1$ m. It may be notice that amplitudes of elevation obtained by the compressible model are higher than those of incompressible model, while the inverse occurs for amplitudes of pressure. Differences of heights of elevation are 0.055 m that corresponds a height, obtained by compressible model, 7.9% higher than incompressible one. Differences of heights of pressure are 1.18 kPa, which represents a pressure height, obtained by compressible model, 12.4% lower than incompressible one. These differences are expected, since the air compressibility input a spring effect that allows a higher displacement of the free surface inside the chamber. Positive amplitudes of both elevation and pressure are higher than negative ones for incompressible model that occur due to non-linear effects of the fluid-structure interaction. These differences are increased for compressible model, because of different behavior between inhalation and exhalation of the air.

Temporal series of elevation and pressure inside the chamber for incident wave with $T = 9$ s and $H = 2$m are shown in Fig. 6. In general, the behavior of temporal series of elevation and pressure for an incident wave with $H = 2$ m is similar to those obtained for wave with $H = 1$ m. Except the fact that the compressibility effect for incident wave with $H = 2$ m imposes a non-linearity with higher significance during the inhalation than that observed in the case with wave 1 m high. The height obtained by compressible model is 0.126 m (9.0%) greater than that of incompressible model. The pressure height of compressible model is 1.61 kPa (8.5%) lower than that of incompressible one. These percentage differences are in the same order of magnitude of those for incident wave with $H = 1$m.

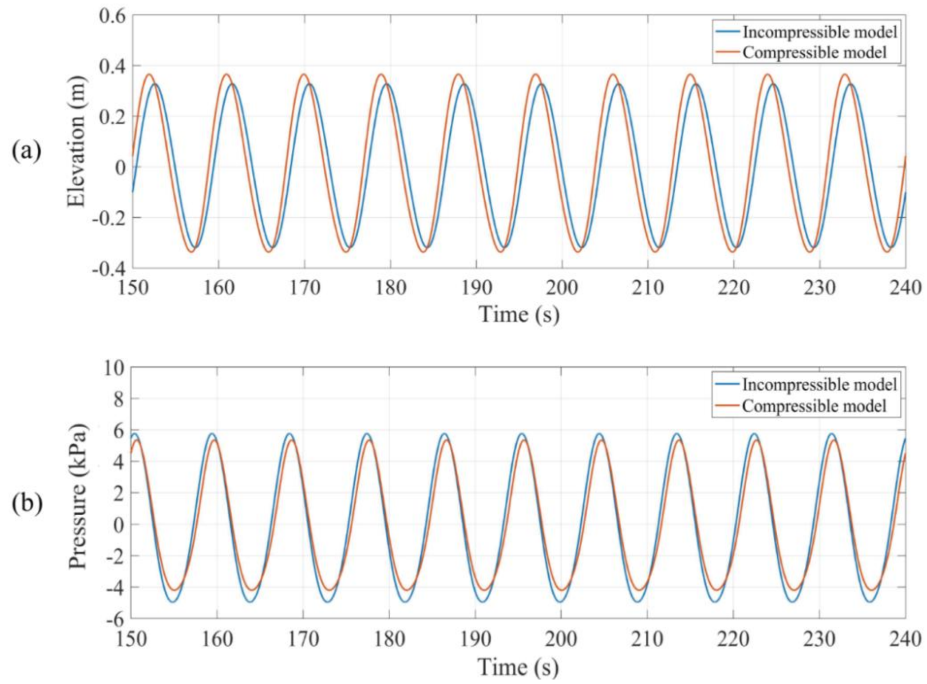

Figure 5. Temporal series of (a) free surface elevation and (b) pressure inside the chamber for incident wave with *T* = 9 s and *H* = 1 m.

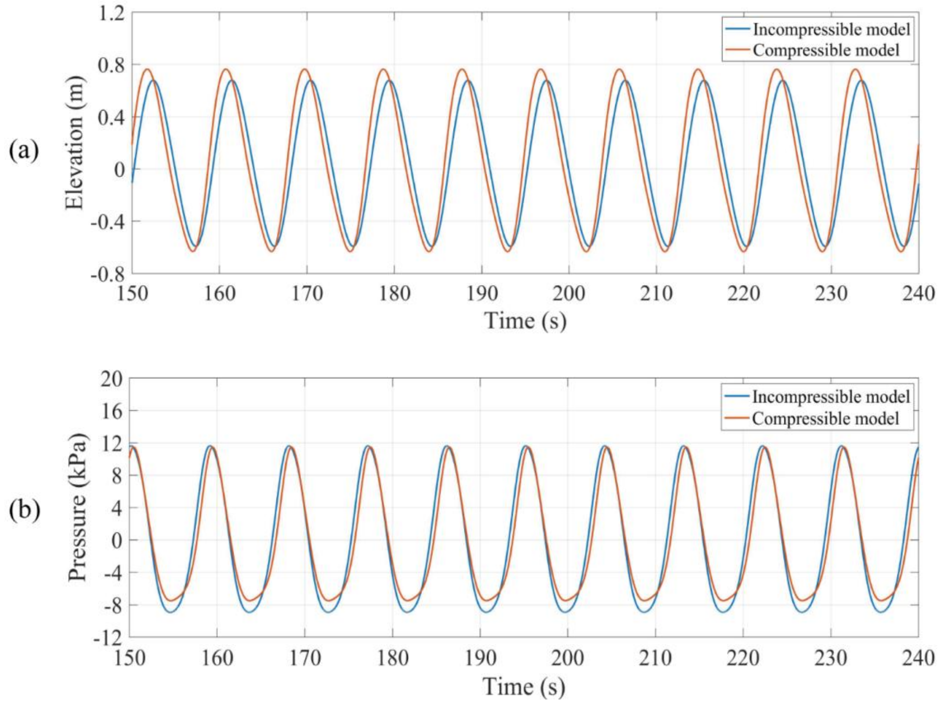

Figure 6. Temporal series of (a) free surface elevation and (b) pressure inside the chamber for incident wave with *T* = 9 s and *H* = 2 m.

Temporal series of flow rate of the turbine for both incident waves (H = 1 and 2 m) are shown in Fig. 7. Differences of behaviors between flow rates obtained by compressible and incompressible models are similar to those of pressure (Fig. 5b and 6b). The pressure and the turbine flow rate are in phase, as expected. The phase between the elevation and the flow rate is 2.15 s considering an incompressible air. This value is approximately T/4 (2.25 s), which is the phase between the elevation and its derivate that, in this case, is proportional to the flow rate if the signal is sinusoidal for incompressible flow. This phase changes when compressible model is used for 1.23 s, because of the air compressibility effect that acts as a spring.

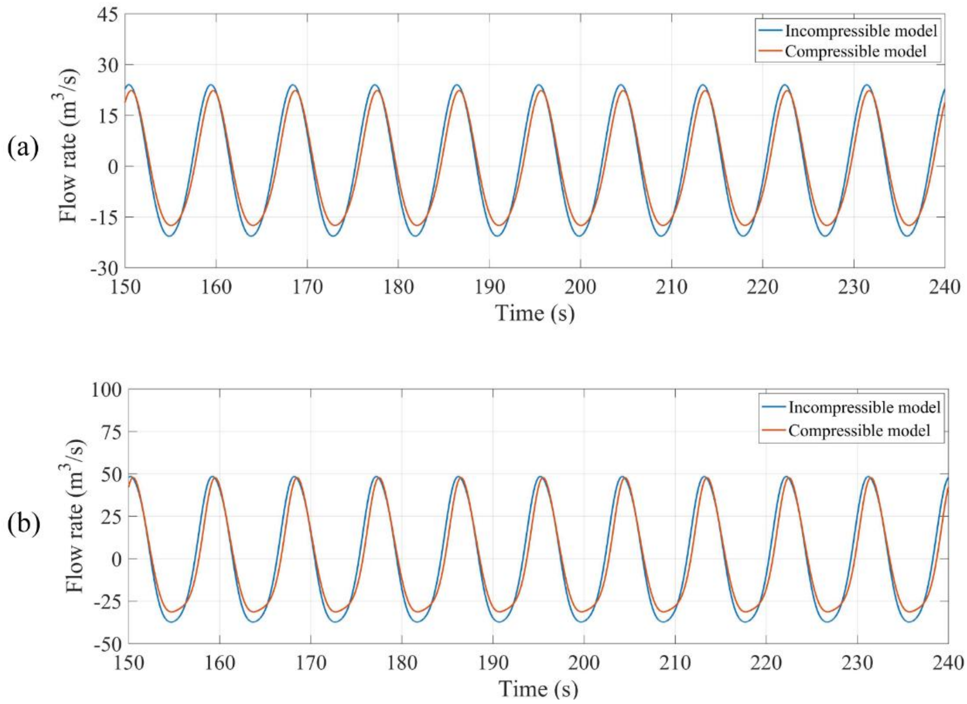

Figure 7. Temporal series of flow rate of the turbine for incident waves with *T* = 9 s and (a) *H* = 1 m and (b) *H* = 2 m.

Figure 8 shows temporal series of pneumatic powers (P_p) obtained for incident waves with H = 1 and 2 m. Mean values of pneumatic power ($\bar{P}_p$), incident wave power ($\bar{P}_w$) and efficiency (η), for both cases, are shown in Tab. 1, where η is the percentage of $\bar{P}_p$ in relation to $\bar{P}_w$. The asymmetries (between positive and negative values) observed in temporal series of elevation and pressure result in a pneumatic power amplitude during the inhalation much lower than that of the exhalation process. These differences are intensified considering compressible effects, which intensify non-linearity phenomena during the inhalation.

Efficiencies obtained for both cases (H = 1 and 2 m) are very similar, that is around 50% for compressible model and 63% for incompressible model. It shows the low influence of the wave height on the efficiency, although, it is expected that, for heights higher than 2 m, can occur wave breaking on the front wall and, consequently a decrease of efficiency. However, results of compressible model are about 21% lower than those obtained by incompressible model. This fact shows the importance of considering the compressibility effects in the models to have accuracy in the device design.

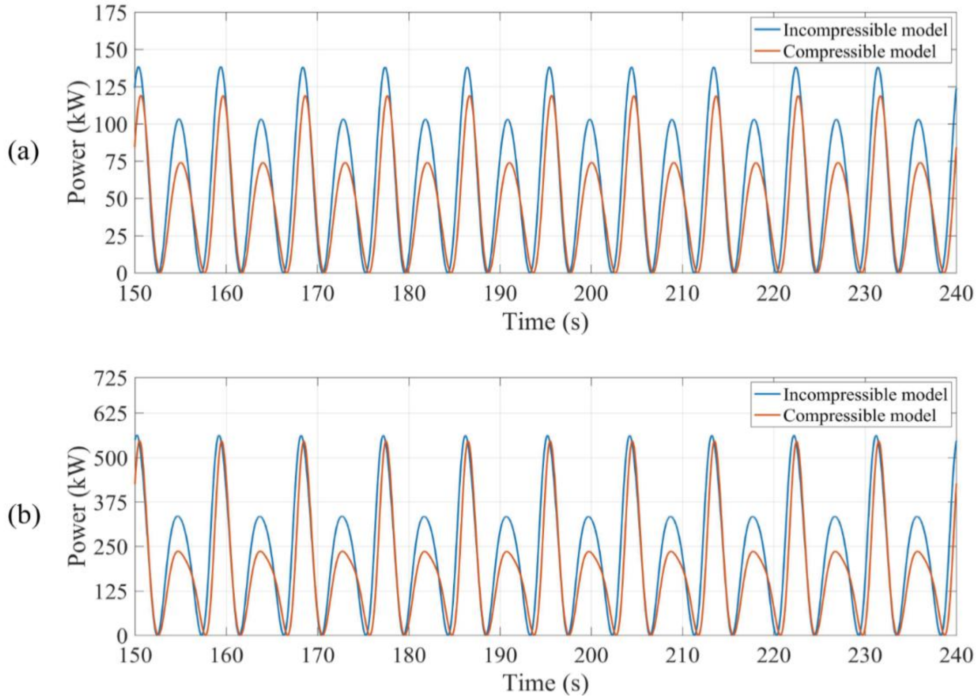

Figure 8. Temporal series of pneumatic power for incident waves with *T* = 9 s and (a) *H* = 1 m and (b) *H* = 2 m.

Table 1. Mean values of pneumatic power and wave power.

***H* (m)**	$\bar{P}_w$ **(kW)**	$\bar{P}_p$ **(kW)**		***η* (%)**	
		Incompressible Model	Compressible Model	Incompressible Model	Compressible Model
1.0	94.3	61.0	47.6	64.7	50.5
2.0	377.3	233.2	186.5	61.8	49.4

Figure 9 shows the vorticity magnitude and streamlines during a wave period (9 s) at nine instants for wave height equal to 1 m obtained by compressible model. The first plate (time = 0) is related to the up zero up-crossing of free surface elevation inside the chamber. It can be seen that the oscillation of free surface outside and inside the front wall are not in phase. In all instants, streamlines are well behaved, possibly because the low wave height and the high value of turbine characteristic relation that impose restrictions to the oscillation of the free surface inside the chamber. The higher vorticity magnitudes are located around an inferior little part of the frontal wall (maximum of 6.1 s^{-1}). It indicates that the viscous effect in the water is not significant in practically all regions for this case.

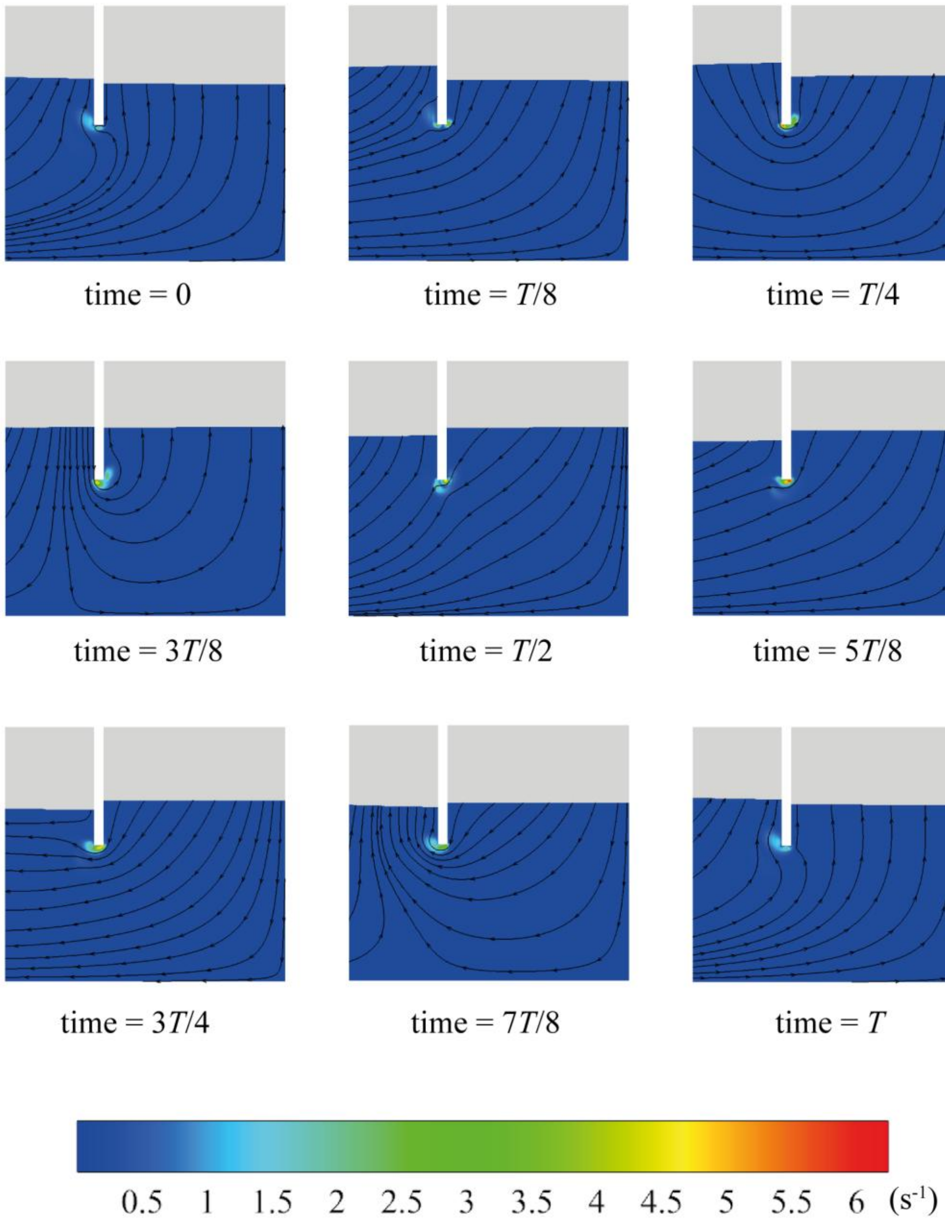

Figure 9. Vorticity magnitude and streamlines during a wave period for incident wave with *T* = 9 s and *H* = 1 m.

5 CONCLUSIONS

In this study, the compressibility effect of the air inside the chamber of an onshore OWC device was analysed by using FLUENT® RANS-VoF model. Two cases, with incident waves with period of 9 s and heights of 1 and 2 m, are investigated. The turbine is Wells-type with a turbine characteristic relation of 240 Pa s m^{-3}. Results of two models are compared: incompressible and compressible models. The former consider the air flow inside the chamber as incompressible one and the later takes into account the effect of the compressibility of the air considering an adiabatic process and the state equation of an ideal gas.

The free surface elevation inside the chamber obtained by compressible model is higher (differences in the height in 0.055 and 0.126 m for incident waves of $H = 1$ and 2 m, respectively) than that of incompressible model; the inverse occurs for air pressure (differences in the height of pressure in 1.18 and 1.61 kPa for H = 1 and 2 m, respectively). This behavior is expected due to the spring effect imposed by air compressibility.

Efficiencies obtained for both cases (H = 1 and 2 m) are very similar, that is around 50% for compressible model and 63% for incompressible model. These values indicate that efficiencies of the compressible model are about 21% lower than those obtained by incompressible model.

The methodology of this study enables the use of a RANS-VoF model to evaluate the performance of OWC devices taking into account the compressibility effects of the air inside the chamber. This investigation shows that the air compressibility has significant influence on the OWC performance.

Acknowledgements

The authors acknowledge the support of Universidade Federal do Rio Grande. The first author acknowledges the support of CNPq (Conselho Nacional de Desenvolvimento Científico e Tecnológico) for the post-graduate scholarship.

REFERENCES

Bouali, B., & Larbi, S., 2017. Sequential optimization and performance prediction of an oscillating water column wave energy converter. *Ocean Engineering*, vol. 131, pp. 162-173.

Brito-Melo, A., Gato, L. M. C., & Sarmento, A. J. N. A, 2002. Analysis of Wells turbine design parameters by numerical simulation of the OWC performance. *Ocean Engineering*, vol. 29, n. 12, pp. 1463-1477.

Das, T. K., Halder, P., & Samad, A., 2017. Optimal design of air turbines for oscillating water column wave energy systems: A review. *The International Journal of Ocean and Climate Systems*, vol. 8, n. 1, pp. 37-49.

Day, A. H., Babarit, A., Fontaine, A., He, Y. -P., Kraskowski, M., Murai, M., Penesis, I., Salvatore, F., Shin, & H. -K., 2015. Hydrodynamic modelling of marine renewable energy devices: A state of art review. *Ocean Engineering*, vol. 108, pp. 46-69.

Dean, R. G., Dalrymple, R. A, 2000. *Water wave mechanics for engineers and scientists*. World scientific publishing Co. Pte. Ltd., London.

Dias, J., Mendonça, A., Didier, E., Neves, M.G., Conde, J.M.P., & Teixeira, P.R.F., 2015. Application of URANS-VOF models in hydrodynamics study of oscillating water column. In: *Proceedings of SCACR2015 – International Short Course/Conference on Applied Coastal Research*, Florence, Italy.

Didier, E., Paixão Conde, J.M., & Teixeira, P.R.F., 2011. Numerical simulation of an oscillation water column wave energy converter with and without damping. In: *Proceedings of the fourth International Conference on Computational Methods in Marine Engineering*, Lisbon, pp. 206-217

Didier, E., Teixeira, P. R. F., & Neves, M. G., 2017. A 3D Numerical Wave Tank for Coastal Engineering Studies. *Defect and Diffusion Forum*, vol. 372, pp. 1-10.

Falcão, A. F. O., 2010. Wave energy utilization: A review of the technologies. *Renewable and Sustainable Energy Reviews*, vol. 14, n. 3, pp. 899-918.

Falcão, A. F. O, 2002. Control of an oscillating-water-column wave power plant for maximum energy production. *Applied Ocean Research*, vol. 24, n. 2, pp. 73-82.

Falcão, A. F. O., & Henriques, J. C. C, 2015. Oscillating-water-column wave energy converters and air turbines: A review. *Renewable Energy*, vol. 85, pp. 1391-1424.

FLUENT, 2007. Version 6.3.16 – User's Guide. ANSYS Inc.

Hirt, C. W., & Nichols, B. D., 1981. Volume of fluid (VOF) method for the dynamics of free boundaries. *Journal of computational physics*, vol. 39, pp. 201-225.

Horko, M., 2007. *CFD optimization of an oscillating water column wave energy converter*. Degree of 500 Master of Engineering Science, School of Mechanical Engineering, Faculty of Engineering, 501 Computing and Mathematics, The University of Western Australia.

International Energy Agency, 2008. *World Energy Outlook*, pp. 140-157.

International Energy Agency, 2015. *World Energy Outlook*. pp. 25-33.

Iturrioz, A., Guanche, R., Lara, J.L., Vidak, C., & Losada, I.J., 2015. Validation of OpenFoam® for oscillating water column three-dimensional modeling. *Ocean Engineering*, 107, pp. 222-236.

Jossét, C., & Clément, A. H., 2007. A time-domain numerical simulator for oscillating-water-column wave power plants. *Renewable Energy*, vol. 32, n. 8, pp. 1379-1402.

Kamath, A., Bihs, H., & Arntsen, Ø., 2015. Numerical modeling of power take-off damping in an oscillating water column device. *International Journal of Marine Energy*, 10, pp. 1-16.

Liu, Z., Hyun, B.S., & Hong, K.Y., 2008. Application of numerical wave tank to OWC air chamber for wave energy conversion. In: *Proceedings of the 18th International Offshore and Polar Engineering Conference, Vancouver*, pp. 350-356.

Liu, Z., Hyun, B., Hong, K., & Lee, Y., 2009a. Investigation on integrated system of chamber a for OWC wave energy convertor. In: *Proceedings of the Nineteenth International Offshore Engineering Conference*, Osaka.

Liu, Z., Shi, H., & Hyun, B., 2009b. Practical design and investigation of the breakwater OWC facility in China. In: *Proceedings of the 8th European Wave and Tidal Energy Conference*, Uppsala.

Lopéz, I., Pereiras, B., Castro, F., & Iglesias, G., 2014. Optimisation of turbine-induced damping for an OWC wave energy converter using a RANS-VOF numerical model. *Applied Energy*, vol. 127, pp. 105-114.

Lopéz, I., Pereiras, B., Castro, F., & Iglesias, G., 2016. Holistic performance analysis and turbine-induced damping for an OWC wave energy converter. *Renewable Energy*, vol. 85, pp. 1155-1163.

Medina-López, E., Moñino, A., Borthwick, A. G. L., & Clavero, M., 2017. Thermodynamics of an OWC containing real gas. *Energy*, vol. 135, pp. 709-717.

Mendonça, A., Dias, J., Didier, E., Fortes, C.J.E.M., Neves, M.G. Reis, M.T., Conde, J.M.P., Poseiro, P., & Teixeira, P.R.F., 2017. An integrated tool for modelling OWC-WECs in vertical breakwaters: preliminary developments. *Journal of Hydro-environment Research*. ISSN 1570-6443. Accepted to be published.

Mørk, G., Barstow, S., Kabuth, A., & Pontes, M. T., 2010. Assessing the global wave energy potential. In: Proceedings of *ASME 2010 29th International Conference on Ocean, Offshore and Arctic Engineering* (OMAE2010-20473), pp. 447-454.

Pereiras, B., Lópes, I., Castro, F., & Iglesias, G., 2015. Non-dimensional analysis for matching an impulse turbine to an OWC with an optimum energy transfer. *Energy*, vol. 87, pp. 481-489.

Paixão Conde, J.M., Teixeira, P.R.F., & Didier, E., 2011. Numerical simulation of an oscillating water column wave energy converter: Comparison of two numerical codes. In: *Proceedings of the 21th International Offshore and Polar Engineering Conference*, Maui, pp. 688-674.

Raghunathan, S., 1995. The Wells air turbine for wave energy conversion. *Progress in Aerospace Sciences*, vol. 31, pp. 335-386.

Setoguchi, T., Santhakumar, S., Maeda, H., Takao, M., & Kaneko, K., 2001. A review of impulse turbines for wave energy conversion. *Renewable Energy*, vol. 23, n. 2, pp. 261-292.

Setoguchi, T., & Takao, M., 2006. Current status of self-rectifying air turbines for wave energy conversion. *Energy conversion & management*, vol. 47, n. 15-16, pp. 2382-2396.

Sheng, W., Alcorn, R., & Lewis, A., 2013. On thermodynamics in the primary power conversion of oscillating water column wave energy converters. *Journal of Renewable and Sustainable Energy*, vol. 5, n. 2.

Sheng, W., & Lewis, A., 2016. Wave energy conversion of oscillating water column devices including air compressibility. *The International Journal of Ocean and Climate Systems*, vol. 8, n. 5.

Teixeira P. R. F., Davyt, D. P., Didier, E., & Ramalhais, R., 2013. Numerical simulation of an oscillating water column device using a code based on NaviereStokes equations. *Energy*, vol. 61, n. 1, pp. 513–530.

Torres, F. R., 2015. *Método numérico simplificado para determinação das curvas de potência mecânica de turbina Wells instalada em dispositivo para captação da energia das ondas do tipo coluna de água oscilante sob incidência de ondas monocromáticas*. Master thesis, Universidade Federal do Rio Grande.

Torres, F. R., Teixeira, P. R. F., & Didier, R., 2016. Study of the turbine power output of an oscillating water column device by using a hydrodynamic - Aerodynamic coupled model. *Ocean Engineering*, vol. 125, pp. 147-154.